Available online at www.sciencedirect.com
ScienceDirect
Journal of Sound and Vibration 324 (2009) 107–125
JOURNAL OF SOUND AND VIBRATION
www.elsevier.com/locate/jsvi

Numerical and experimental investigations of flexural vibrations of a rotor system with transverse or slant crack

Yanli Lin*, Fulei Chu

Department of Precision Instruments and Mechanology, Tsinghua University, Beijing 100084, China

Received 16 June 2008; received in revised form 28 November 2008; accepted 24 January 2009
Handling Editor: L.G. Tham
Available online 6 March 2009

Abstract

Flexural vibrations of a rotor system with transverse or slant crack are analyzed under torsional excitation by numerical simulation and experiment. Numerical results show that combination frequencies of the rotating speed and the torsional excitation frequency are prominent in the flexural responses of a slant-cracked rotor, but too weak to be identified for a transverse-cracked rotor. In order to verify the results, an experimental setup is installed to simulate the cracked rotor system and a special structure is designed to exert the torsional excitation on the cracked rotor. The experimental results present almost identical characteristic features about the combination frequencies to the numerical results. The numerical and experimental investigations demonstrate these features can be used to distinguish between the transverse crack and the slant crack on the shaft of a rotor system.
© 2009 Elsevier Ltd. All rights reserved.

1. Introduction

Crack is one of classic malfunctions in the rotor system. If undetected timely, crack might result in destructive failure. People have realized the severity of crack failures long ago. Since the 1970s, investigations on the cracked rotors [1,2] have been undertaken. Initially, almost all works concentrated on the transverse-cracked rotor. Dimarogonas [3] thoroughly presented those study results and bibliographies which were published from 1970s to 1990s in his comprehensive reference. However, in the actual situation there exists the slant crack resulted from the fatigue of the shaft due to an excessive torsional moment, in contrast to the transverse crack due to an excessive bending moment. For example, Fig. 1 displays a slant-cracked shaft in an aeroengine [4]. It can be seen that a crack about 45° towards the axis of the shaft is adjacent to the torque transmission part. The analysis results showed that poor manufacturing technique and excessive torsional moments led to the slant crack. Because a lot of rotor systems are used to transfer torsional moments, it is almost inevitable that the slant crack occurs on the shafts of those rotor systems.

In fact, early in the 1980s, Ichimonji [5,6] had made the research on the dynamics of a rotor system with a slant crack on the shaft. Motion equations in his researches only involved two flexural directions and were

*Corresponding author.
E-mail address: lin-y103@mails.tsinghua.edu.cn (Y. Lin).

0022-460X/$ - see front matter © 2009 Elsevier Ltd. All rights reserved.
doi:10.1016/j.jsv.2009.01.058

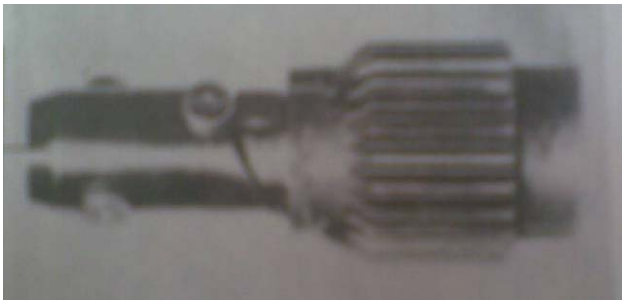

Fig. 1. Slant-cracked transmission shaft on the aeroengine.

obtained on the assumption that the stiffness of the slant-cracked shaft oscillated synchronously with the torsional vibration. One of his conclusions was that torsional excitation made the steady-state responses of two flexural directions contain rotating speed, twice of the rotating speed and subharmonic frequencies at intervals of torsional frequency centered at the rotating speed and twice of the rotating speed. Recently, Indian scholars Sekhar et al. [7,8] began to discuss the dynamic behaviors of the rotor system with a slant crack on the shaft. FEM was used to establish motion equations of the slant-cracked rotor system. Sekhar obtained similar conclusions to those of Ichimonji's. However, his paper [8] about transverse crack versus slant crack, which presented all his main works in the recent decade, did not put up the flexural responses of the transverse-cracked shaft considering the torsional moment. The comparison between the flexural responses of the transverse-cracked rotor and the slant-cracked one needs to be studied further. In the year of 1997, Indian scholar Darpe investigated the slant-cracked rotor with three [9] and four [10] degrees of freedom which included two flexural, one torsional and one axial directions using FEM. He discussed in detail the influence of the orientation of the slant crack on the stiffnesses and investigated the responses of the slant-cracked shaft and the transverse-cracked one with or without the torsional excitation. He concluded that "Comparing the amplitudes of torsional excitation frequency in vertical and horizontal directions in lateral vibration spectra, it is possible to detect the type of crack-transverse or slant". All these scholars made great contributions to the study of the slant crack on the shaft, and all their numerical results indicated that combination frequencies of the rotating speed and the torsional excitation frequency in flexural responses may be used to discriminate between the transverse crack and the slant one on a rotor shaft.

In the following sections of this paper, motion equations of a cracked rotor system under torsional excitation will be established with four degrees of freedom including two flexural directions, one torsional direction and one axial direction. Stiffnesses of four directions will be derived. Then these equations will be solved using Runge–Kutta method. Numerical results of the transverse-cracked rotor and the slant-cracked one will be compared. Afterwards, an experimental setup will be introduced to simulate the transverse-cracked rotor and the slant-cracked one under the torsional excitation. And experimental results will be analyzed and compared. Finally, some conclusions will be drawn.

2. Motion equations

The rotor system investigated is a Jeffcott rotor system as shown in Fig. 2(a), with a 45° slant crack or a transverse crack adjacent to the disk. In Fig. 2(b), xoy is a stationary coordinate system, $\xi o\eta$ is a rotating coordinate system, and $\xi' o' \eta'$ is a coordinate system fixed with the disk, o' is the center of the disk, C is the mass center, φ is the phase angle of the mass center, Ω is the rotating speed, α is the angle caused by the torsional vibration, and t is the time. Therefore $\Omega t + \alpha$ is the total rotatory angle of the disk.

Motion equations of the rotor system with two flexural directions, one torsional direction and one axial direction can then be expressed as

$$m\ddot{x} + c\dot{x} + k_x x + k_{xy} y + k_{xT}\alpha + k_{xu} u = -mg + me(\Omega + \dot{\alpha})^2 \cos(\Omega t + \alpha + \varphi) + me\ddot{\alpha} \sin(\Omega t + \alpha + \varphi) \quad (1)$$

$$m\ddot{y} + c\dot{y} + k_{xy} x + k_y y + k_{yT}\alpha + k_{yu} u = me(\Omega + \dot{\alpha})^2 \sin(\Omega t + \alpha + \varphi) - me\ddot{\alpha} \cos(\Omega t + \alpha + \varphi) + A \sin(\omega_T t) \quad (2)$$

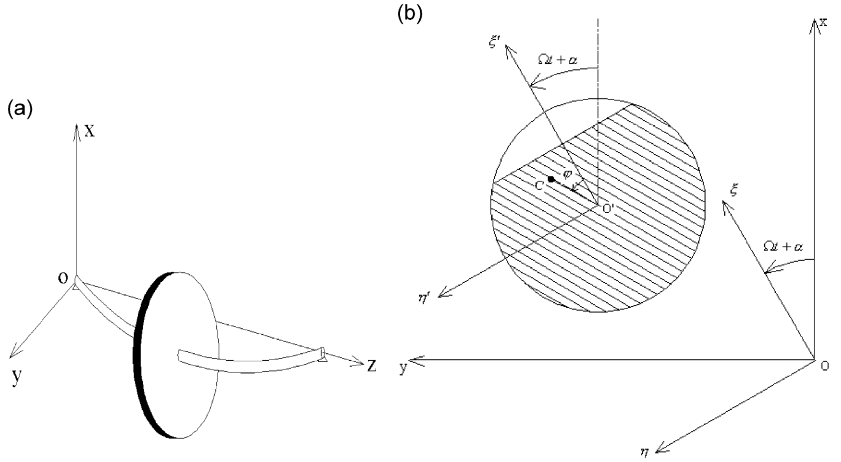

Fig. 2. Jeffcott rotor system with three coordinate systems: (a) Jeffcott rotor model and (b) projection of the crack cross section along z-direction.

$$J_p\ddot{\alpha} + c_T(\Omega + \dot{\alpha}) + k_{xT}x + k_{yT}y + k_T\alpha + k_{Tu}u = B\sin(\omega_T t) + C + mge\sin(\Omega t + \alpha + \varphi) + m\ddot{x}e\sin(\Omega t + \alpha + \varphi) - m\ddot{y}e\cos(\Omega t + \alpha + \varphi) \quad (3)$$

$$m\ddot{u} + c_u\dot{u} + k_{xu}x + k_{yu}y + k_{Tu}\alpha + k_u u = 0 \quad (4)$$

where m is the mass of the disk, J_p the moment of inertia, c, c_T and c_u are the damping coefficients of flexural, torsional and axial vibrations, respectively. x, y, α, u are, respectively, the vertical and horizontal flexural displacements, the torsional angle, and the axial displacement.

$$[k]_g = \begin{bmatrix} k_x & k_{xy} & k_{xT} & k_{xu} \\ k_{xy} & k_y & k_{yT} & k_{yu} \\ k_{xT} & k_{yT} & k_T & k_{Tu} \\ k_{xu} & k_{yu} & k_{Tu} & k_u \end{bmatrix}$$

is the stiffness matrix which will be discussed in detail in the next section, e is the mass eccentricity of the disk, i.e. the length of $o'C$ in Fig. 2(b). ω_T is the frequency of torsional excitation and B the amplitude of the torsional excitation. C is a torque constant. In Eq. (2), there is one term: $A\sin(\omega_T t)$, which is a horizontal force brought by the torsional excitation considering some real situations. It is identical to the following experimental situations. The above four equations are based on the assumption that there is no axial excitation because in most cases either there is no axial excitation input for the rotor system or the axial excitation can be neglected.

3. Shaft stiffnesses

It is well known that the existence of a crack on the shaft will change the stiffness of the shaft itself. In order to solve Eqs. (1)–(4), the stiffness matrix $[k]_g$ must be determined firstly.

In Fig. 3, there is a transverse crack or a 45° slant crack on the middle position of the shaft. The coordinate system XoY is corresponding to the rotating coordinate system $\xi o\eta$ in Fig. 2. A tensional force q_1, two bending moments q_4 and q_5, and a torsional moment T are exerted on the shaft. It is supposed that $R = d/2$ is the radius of the shaft and a is the depth of the crack. The stiffness of the cracked shaft can then be obtained by the Dimarogonas method [11]. Firstly a thin slice is extracted along the direction perpendicular to Y-axis. According to the stress state of the thin slice, stress intensity factors (SIFs) of the crack can be known according to SIFs for the single edge cracked plate of tension specimen, bending specimen, II type shear specimen or III type shear specimen in Ref. [12]. Then strain energy density function (SEDF) can be obtained

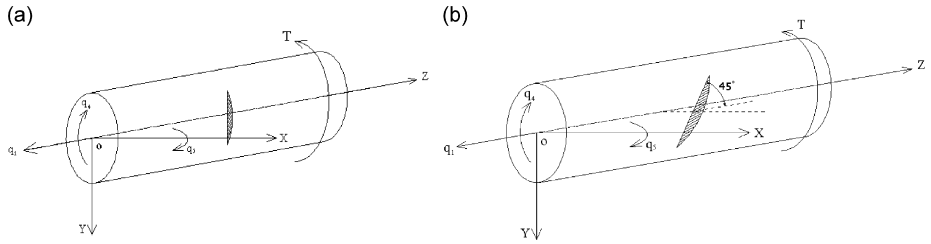

Fig. 3. Shaft with a transverse or slant crack under four loads: (a) shaft with a transverse crack and (b) shaft with a slant crack.

by the relationship between SIFs and SEDF. By integrating SEDF along the crack area, the released strain energy due to the whole crack can be obtained. The second-order derivatives of the released strain energy with respect to loads are additional flexibilities of the shaft with the crack. The additional flexibilities plus the flexibilities of the uncracked shaft are the total flexibilities of the cracked shaft. Stiffnesses can be obtained as the inverse of the total flexibilities.

According to the stress state of the thin slice extracted along the direction perpendicular to Y-axis, SIFs caused by different loads with an arbitrary crack depth γ are given as follows.

For a transverse crack:

$$q_1:\ K_{\mathrm{I}1}=\sigma_1\sqrt{\pi\gamma}F_1 \quad \sigma_1=\frac{q_1}{\pi R^2} \tag{5}$$

$$q_4:\ K_{\mathrm{I}4}=\sigma\sqrt{\pi\gamma}F_1 \quad \sigma=\frac{4q_4Y}{\pi R^4} \tag{6}$$

$$q_5:\ K_{\mathrm{I}5}=\sigma\sqrt{\pi\gamma}F_2 \quad \sigma=\frac{4q_5\dfrac{h}{2}}{\pi R^4} \tag{7}$$

$$T:\ K_{\mathrm{III}T}=\tau\sqrt{\pi\gamma}F_{\mathrm{III}} \quad \tau=\frac{2T\sqrt{Y^2+\left(\dfrac{h}{2}\right)^2}}{\pi R^4} \tag{8}$$

For a slant crack:

$$q_1:\ K_{\mathrm{I}1}=\sigma_1\sqrt{\pi\gamma}F_1 \quad \sigma_1=\frac{q_1}{2\pi R^2} \tag{9}$$

$$K_{\mathrm{III}1}=\tau_1\sqrt{\pi\gamma}F_{\mathrm{III}} \quad \tau_1=\frac{q_1}{2\pi R^2} \tag{10}$$

$$q_4:\ K_{\mathrm{I}4}=\sigma\sqrt{\pi\gamma}F_1 \quad \sigma=\frac{2q_4Y}{\pi R^4} \tag{11}$$

$$q_5:\ K_{\mathrm{I}5}=\sigma\sqrt{\pi\gamma}F_2 \quad \sigma=\frac{2q_5\dfrac{h}{2}}{\pi R^4} \tag{12}$$

$$K_{\mathrm{III}5}=\tau\sqrt{\pi\gamma}F_{\mathrm{III}} \quad \tau=\frac{2q_5\dfrac{h}{2}}{\pi R^4} \tag{13}$$

$$T:\ K_{IT}=\sigma\sqrt{\pi\gamma}F_2 \quad \sigma=\frac{2T\sqrt{Y^2+\left(\frac{h}{2}\right)^2}}{\pi R^4} \tag{14}$$

where K_I and K_{III} are the crack SIFs corresponding to I and III crack modes, $h=2\sqrt{R^2-Y^2}$.

For the slant crack, because the bending load q_4 can make the upper-half crack close and compressive and the lower-half crack open and tensile, distribution of the shear stress τ along the whole slant crack surface is antisymmetric, and the total shear effect is zero. Therefore, q_4 cannot cause the III crack mode.

For the transverse crack, the total SIFs are

$$K_{III}=K_{IIIT}=\frac{2T\sqrt{Y^2+\left(\frac{h}{2}\right)^2}}{\pi R^4}\sqrt{\pi\gamma}F_{III} \tag{15}$$

$$K_I=K_{I1}+K_{I4}+K_{I5}=\frac{q_1}{\pi R^2}\sqrt{\pi\gamma}F_1+\frac{4q_4Y}{\pi R^4}\sqrt{\pi\gamma}F_1+\frac{4q_5\frac{h}{2}}{\pi R^4}\sqrt{\pi\gamma}F_2 \tag{16}$$

For the slant crack, the total SIFs are

$$K_{III}=K_{III1}+K_{III5}=\left(\frac{q_1}{2\pi R^2}+\frac{2q_5\frac{h}{2}}{\pi R^4}\right)\sqrt{\pi\gamma}F_{III} \tag{17}$$

$$K_I=K_{I1}+K_{I4}+K_{I5}+K_{IT}=\left(\frac{q_1}{2\pi R^2}+\frac{2q_4Y}{\pi R^4}\right)\sqrt{\pi\gamma}F_1+\left(\frac{2q_5\frac{h}{2}}{\pi R^4}+\frac{2T\sqrt{Y^2+\left(\frac{h}{2}\right)^2}}{\pi R^4}\right)\sqrt{\pi\gamma}F_2 \tag{18}$$

The SEDF is

$$J=\frac{1}{E'}[K_I^2+(1+v)K_{III}^2] \tag{19}$$

By $K_I\geqslant 0$, the opening area of the crack can be defined as A' [13]. Assuming the whole area of the crack is A, if the crack opens totally, $A'=A$. The released strain energy due to the existence of the crack is

$$W=\int\int_{A'}\frac{1}{E'}K_I^2\,\mathrm{d}\gamma\,\mathrm{d}Y+\int\int_{A}\frac{1+v}{E'}K_{III}^2\,\mathrm{d}\gamma\,\mathrm{d}Y \tag{20}$$

where $E'=E$ or $E/(1-v^2)$ for plane stress or plane strain, respectively, E is the modulus of elasticity, v the Poisson ratio, F_1, F_2, and F_{III} are the influential functions [12] of SIFs with respect to the single edge cracked plates of the tension specimen, pure bending specimen and III type shear specimen, respectively. On the assumption that $\lambda=\pi\gamma/2h$, the influential functions can be written as

$$F_1=\sqrt{\frac{\tan\lambda}{\lambda}}[0.752+2.02(\gamma/h)+0.37(1-\sin\lambda)^3]\frac{1}{\cos\lambda} \tag{21}$$

$$F_2=\sqrt{\frac{\tan\lambda}{\lambda}}[0.923+0.199(1-\sin\lambda)^4]\frac{1}{\cos\lambda} \tag{22}$$

$$F_{III}=\sqrt{\frac{\tan\lambda}{\lambda}} \tag{23}$$

According to the Castigliano's theorem, the additional local flexibility is

$$\Delta c_{ij} = \frac{\partial^2 W}{\partial q_i \partial q_j} \tag{24}$$

To calculate the stiffness matrix of the cracked shaft, it is necessary to add the additional local flexibility matrix to the flexibility matrix of the uncracked shaft.

$$[c]_l = [G_1][\Delta c][G_2] + [c_s] \tag{25}$$

where

$$[c_s] = diag\left[\frac{l^3}{48EI} \;\; \frac{l^3}{48EI} \;\; \frac{l}{2EA} \;\; \frac{l}{2GI_p}\right], \quad [G_1] = diag\left[\frac{l}{2} \;\; \frac{l}{2} \;\; 1 \;\; 1\right],$$

$$[G_2] = diag\left[\frac{l}{4} \;\; \frac{l}{4} \;\; 1 \;\; 1\right].$$

Then, under the coordinate system XoY in Fig. 3 or $\xi o\eta$ in Fig. 2 the stiffness matrix can be expressed as

$$[k]_l = [c]_l^{-1} \tag{26}$$

Under the stationary coordinate system xoy, the stiffness matrix can be expressed as

$$[k]_g = [H]^{-1}[k]_l[H] \tag{27}$$

where

$$[H] = \begin{bmatrix} \cos(\Phi) & \sin(\Phi) & 0 & 0 \\ -\sin(\Phi) & \cos(\Phi) & 0 & 0 \\ 0 & 0 & 1 & 0 \\ 0 & 0 & 0 & 1 \end{bmatrix}$$

is the transformation matrix, $\Phi = \Omega t + \alpha$.

From Eqs. (15)–(18), (20) and (24), it can be known that a transverse crack on the shaft can lead to bending–tension coupling stiffnesses of the shaft, and a slant crack can lead to bending–torsion–tension coupling stiffnesses. The reason is that for the transverse crack, the tensional force q_1, the bending moments q_4 and q_5 all can cause I crack mode, however for the slant crack besides the above three loads, the torsional moment T can cause I crack mode too. This can be obviously observed in Eqs. (16) and (18).

It must be mentioned that the derivation of stiffness in six degrees of freedom has been well done in Refs. [9,10]. Derivation process in this paper is about the same as that in the references although only four degrees of freedom are taken into account. The only difference is the stress in SIF caused by torsional moment T. From Ref. [12], it is known that influential function F_2 is applied for the single edge cracked plate of pure bending specimen and in such a case the stress in SIF is the maximal value of the bending normal stress. Ref. [12] also shows that influential function F_{III} is applied for the single edge cracked plate of III type shear specimen and in such a case the stress in SIF is a uniform shear stress. It is believed both in the present paper and Refs. [9,10] that the influential function should adopt F_{III} for a transverse crack and F_2 for a slant crack in the SIF caused by torsional moment T. Only this paper believes it is more reasonable to take the maximal stress value of every thin slice as the stress in SIF caused by torsional moment. In fact, both stresses in this paper and Refs. [9,10] are approximations, because along the thin slice extracted from the crack area the stress distribution caused by torsional moment is not absolutely identical to that in Ref. [12]. Calculation illuminates that there is no much difference in the additional flexibilities caused by these two different stresses, though the magnitude of additional flexibility is influenced a little bit. And there is little effect on the coupling stiffnesses and coupling vibrations.

4. Flexural steady-state responses

To compare flexural vibrations of the transverse-cracked shaft with those of the slant-cracked shaft, Runge–Kutta method is used to solve motion Eqs. (1)–(4). In order to match up to the experiment, assume that the crack is open totally all the time. When the crack is always in opening state during shaft rotating, the stiffness matrix under the rotating coordinate system will not change with the time, but it will if the crack is a breathing one.

Parameters of the rotor system: the disk mass $m = 0.595$ kg, length of the shaft $L = 0.26$ m, the diameter of the shaft $d = 9.5$ mm, the depth of the crack $a = d/2$, the diameter of the disk $dp = 76$ mm, additional mass on the disk $dm = (3e - 3)$kg, the distance between the additional mass and the disk center $lm = 32.75$ mm, the eccentricity of the disk $e = dm \bullet lm/(dm + m) = 0.1643$ mm, the phase angle of the mass center $\varphi = \pi/6$, the modulus of elasticity $E = 210$ GPa, the Poisson ratio $v = 0.3$, three damping coefficients $c = 41.65$ kg/s, $c_T = 0.0091$ kg m^2/s, $c_u = 146.2034$ kg/s, the frequency of torsional excitation $\omega_T = 15$ Hz $= 900$ rev/min, the amplitude of torsional excitation $B = 1$ N m, the torque constant $C = 0.5$ N m, the amplitude of flexural force brought by the torsional excitation $A = 0.1$ N. The flexural natural frequency of the rotor system without any crack is 5928.1 rev/min.

Fig. 4 displays the amplitude–frequency spectra of flexural steady-state responses of the transverse-cracked shaft and the slant-cracked shaft with increase of the rotating speed. It is noticeable that in the paper all exhibited flexural amplitude–frequency spectra are in y-direction since the spectrum in x-direction is basically the same as that in y-direction, except for an obvious torsional excitation frequency appearing in the spectrum of y-direction, but no such frequency in x-direction. This is because the crack is assumed open totally all the time. If the crack is a breathing one, there will be a little difference about the amplitudes corresponding to the frequencies appearing in x- and y-directions. However, the main characteristic frequencies are same for an open crack and a breathing one, especially the combination frequencies of rotating speed and torsional excitation frequency. The response of horizontal flexural direction, i.e. y-direction, is corresponding to the measured direction of the following experiment. Moreover, because the amplitude of frequency Ω goes to such a great extent when the speed is close to natural frequency that the amplitudes of the rest frequencies become unnoticeable in the spectra, as shown in Fig. 4(e) and (f). To investigate all the components in the spectra, two segments are separated from the whole spectra. One range of frequency is less than Ω and the other is more than Ω and not greater than 2Ω, just as shown in Fig. 4(a) and (b), (c) and (d), respectively. In order to show the comparison between the flexural responses of the transverse-cracked shaft and the slant-cracked shaft better, Fig. 5 displays several spectra for different rotating speeds less than the natural frequency.

From Fig. 4, it can be seen that the amplitudes reach their maximums both for frequency Ω and combination frequency $|\Omega - \omega_T|$ at a rotating speed close to the natural frequency 5928.1 rev/min of the rotor system, for frequency 2Ω at a rotating speed close to half natural frequency, and for combination frequency $\Omega + \omega_T$ at about 3500 rev/min. It is obvious that the amplitudes of combination frequencies $|\Omega - \omega_T|$ and $\Omega + \omega_T$ are both much larger in the flexural responses of the slant-cracked shaft than those of the transverse-cracked shaft, as shown in Figs. 4 and 5. Especially when the rotor rotates at a low speed, combination frequencies $|\Omega - \omega_T|$ and $\Omega + \omega_T$ are so prominent in the flexural responses of the slant-cracked shaft that their amplitudes have the same order of magnitude as that of frequency Ω, whereas, these two combination frequencies in the flexural responses of the transverse-cracked shaft is not even visible in the spectra, as shown in Fig. 5. Fig. 4 shows that when the speed exceeds the natural frequency of the rotor, the amplitudes of these two combination frequencies begin to reduce with increase of the rotating speed. Fig. 5 indicates that the ratios of amplitudes of the combination frequencies to that of frequency Ω get smaller and smaller with the speed increasing. Therefore, combination frequencies $|\Omega - \omega_T|$ and $\Omega + \omega_T$ could be used to detect and distinguish the slant and transverse cracks on the shaft, and the proper range of application is in the low speeds.

As for the torsional excitation frequency ω_T in the spectra of the horizontal flexural responses, the amplitude is almost same whichever the rotating speed is and whether the crack is transverse or slant, as shown in Figs. 4 and 5.

Fig. 6 displays the spectra of axial steady-state responses. Obviously, for the slant-cracked shaft the axial responses include frequency Ω and the considerable torsional excitation frequency ω_T. For the transverse-cracked shaft, there is only frequency Ω appearing in the axial responses, while frequency ω_T is too small to be watchable. The phenomenon happens because there are bending–torsion–tension coupling stiffnesses for the slant-cracked shaft, and only bending–tension coupling stiffnesses for the transverse-cracked shaft. It is worthy of noting that the amplitudes of frequencies Ω and ω_T change little with increase of the rotating speed

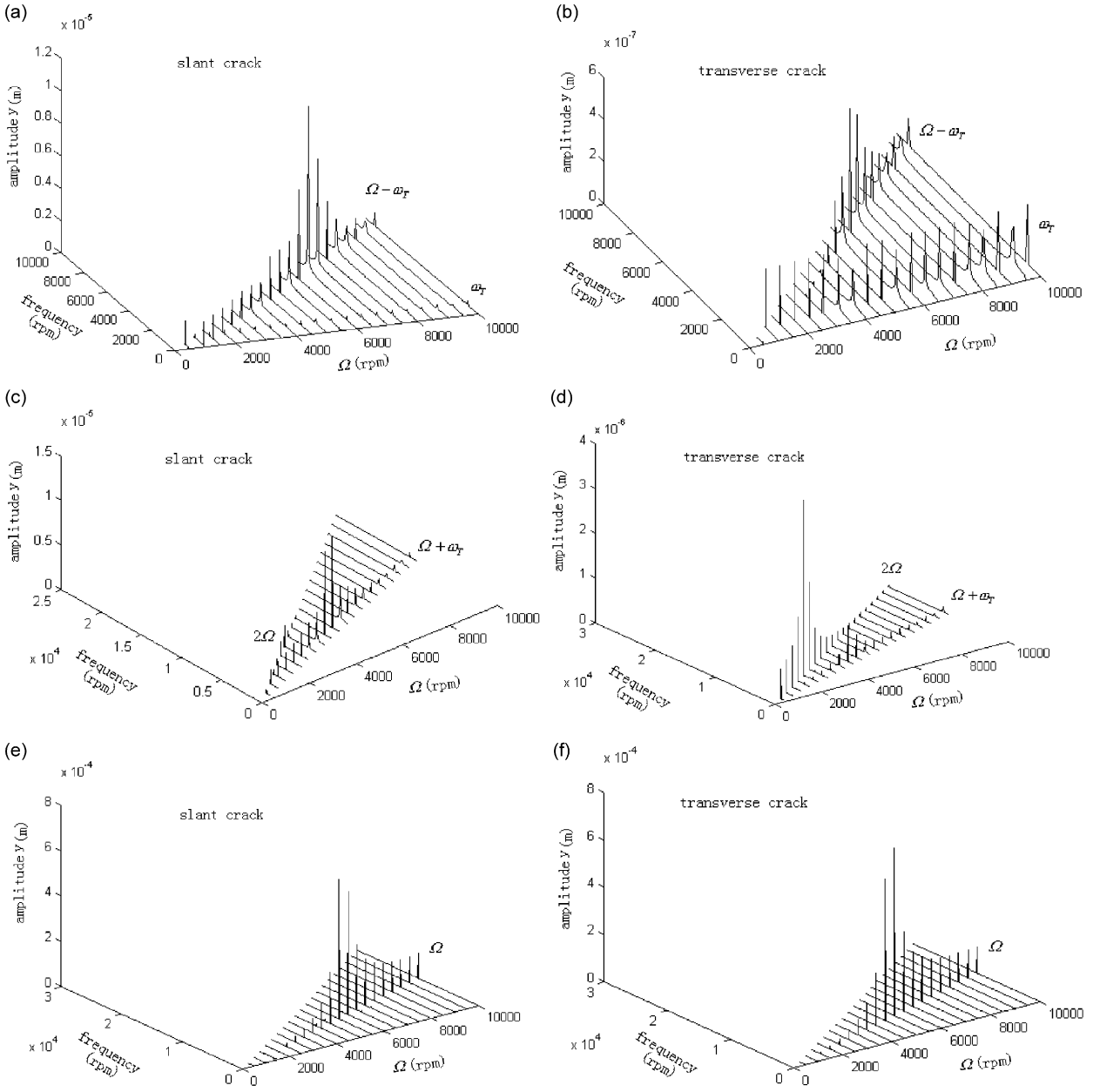

Fig. 4. Amplitude–frequency spectra of steady-state responses of the slant-cracked shaft: (a), (c), (e) or the transverse-cracked shaft and (b), (d), (f) in y-direction.

since these two frequencies are far from the axial natural frequency of the rotor system. Therefore, the distinct torsional excitation frequency ω_T in the axial response is a distinctive characteristic for a slant-cracked shaft, which could be used to distinguish the crack type, transverse or slant, even when the rotating speed exceeds the flexural natural frequency of the rotor system.

From Eqs. (1)–(4), it can be seen that the eccentricity can cause bending–torsion coupling vibration. For the transverse-cracked shaft, since there are bending–tension coupling of the stiffnesses and bending–torsion coupling caused by the eccentricity, tension–torsion coupling will exist as well due to the interaction of couplings. Even then, the slant-cracked shaft manifests much stronger bending–tension–torsion coupling vibrations than the transverse-cracked shaft. The reason is that besides eccentricity causes bending–torsion

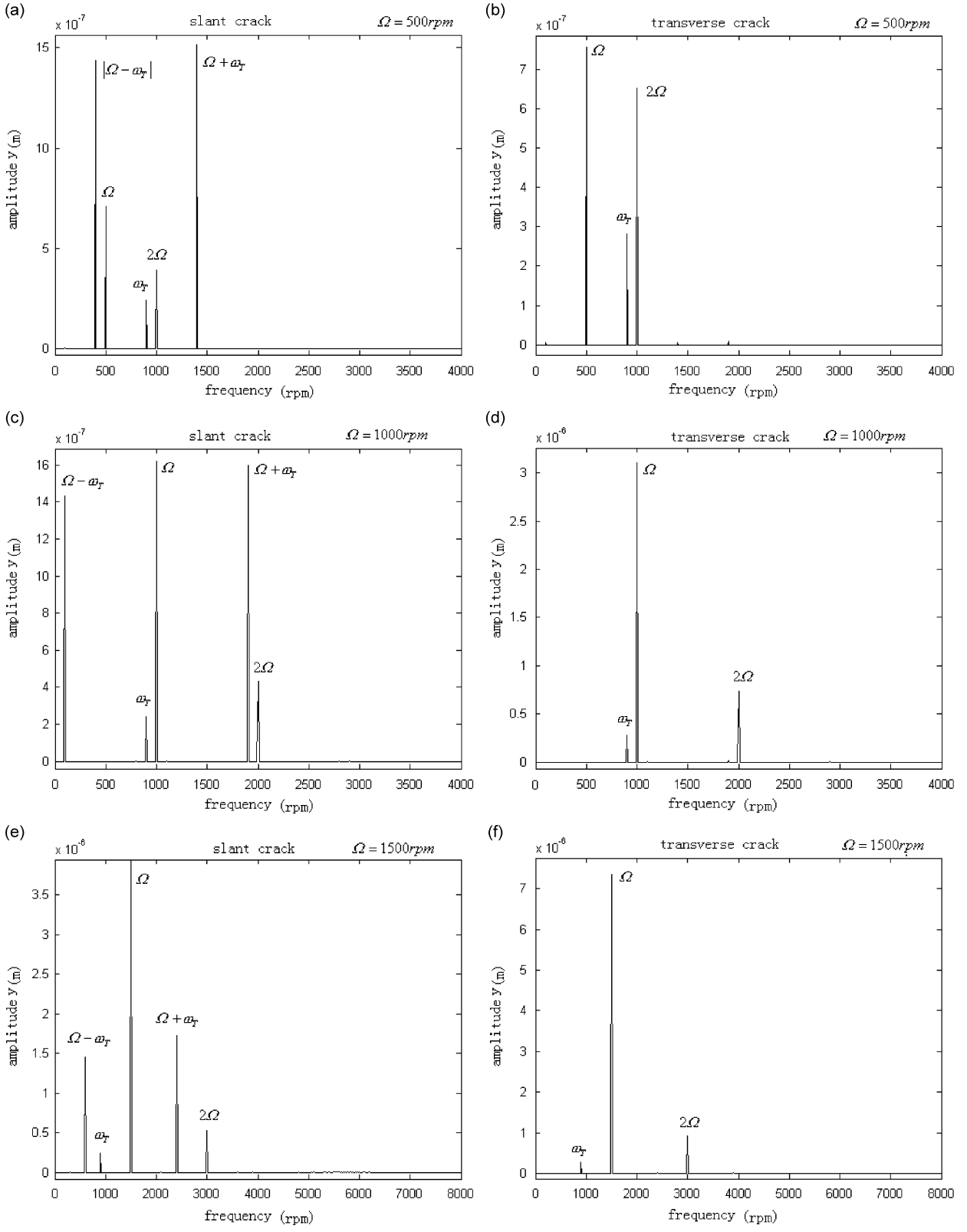

Fig. 5. Spectra of the flexural responses in y-direction with the rotating speeds: 500, 1000, 1500, 2000, 2500, 3000, and 3500 rev/min.

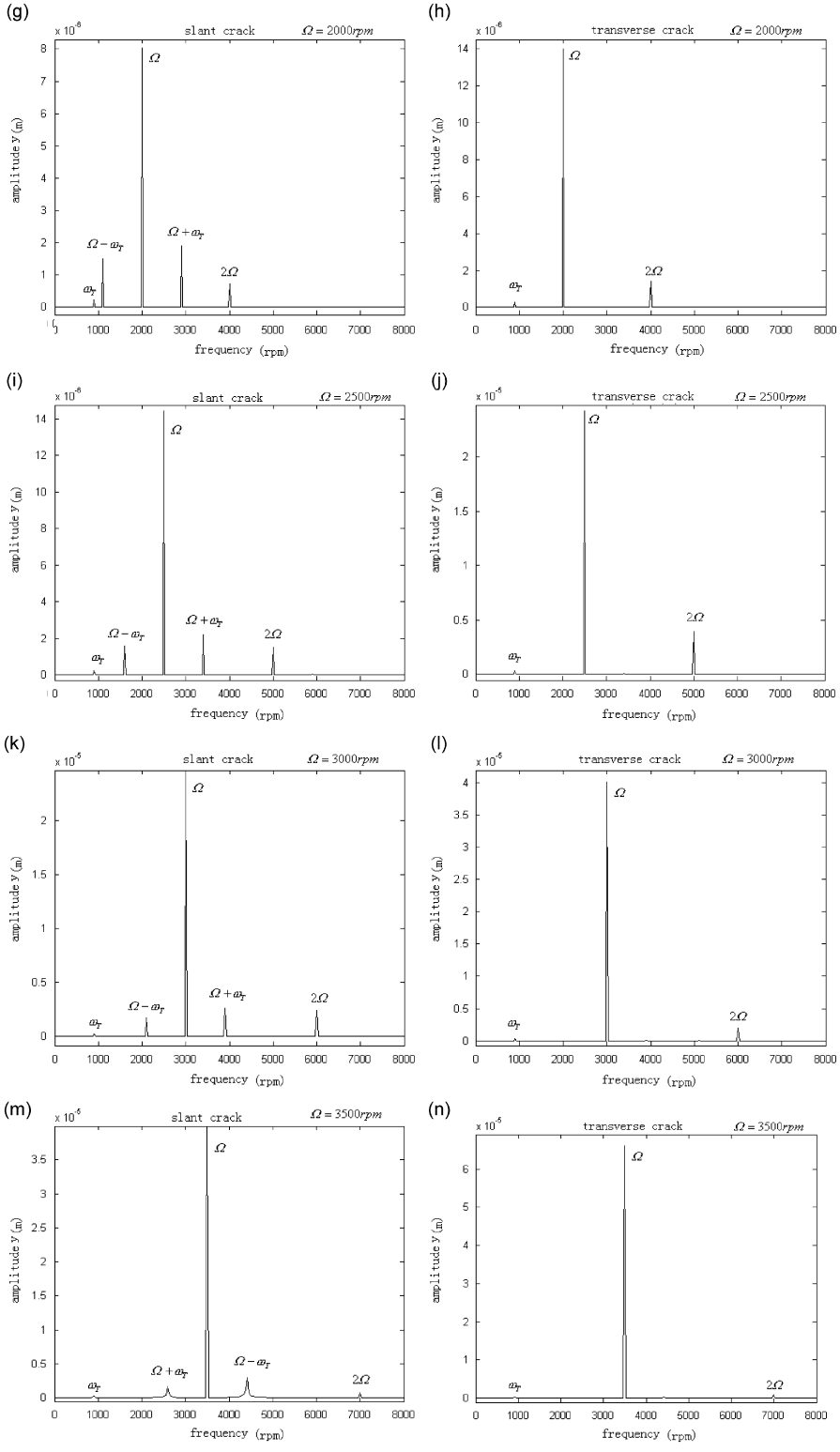

Fig. 5. (*Continued*)

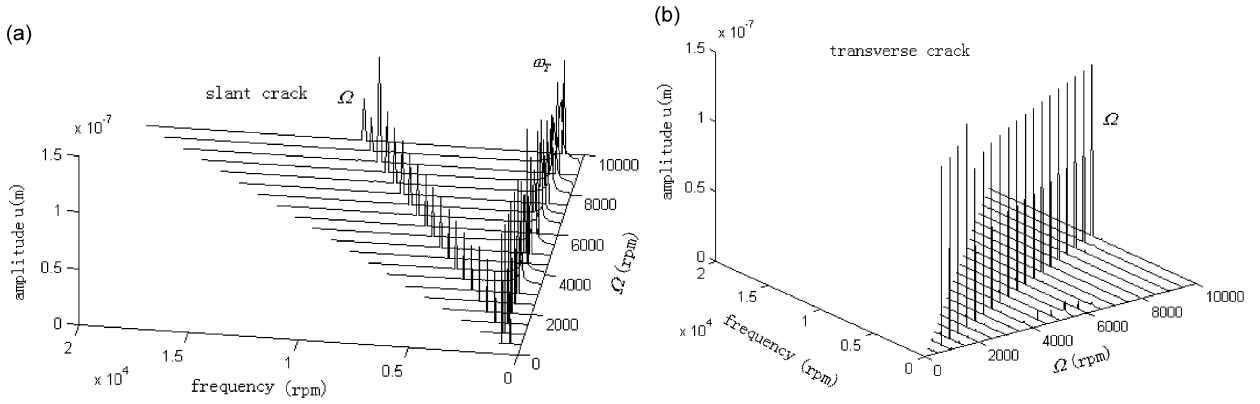

Fig. 6. Amplitude–frequency spectra of axial responses of (a) the slant-cracked shaft: (b) and the transverse-cracked shaft with increase of the rotating speed.

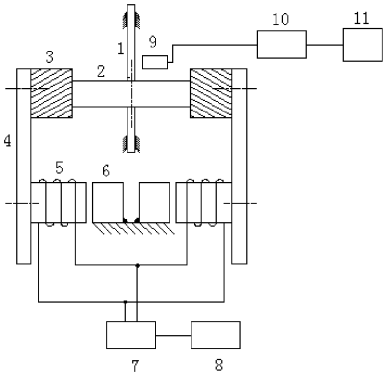

Fig. 7. Schematic diagram of experimental setup: (1) cracked shaft, (2) disk, (3) sliding block, (4) mounting board, (5) electromagnet, (6) ferroferrite, (7) power amplifier, (8) function generator, (9) eddy-current transducer, (10) pre-processor, and (11) computer.

coupling vibrations, there already exist bending–torsion, bending–tension and torsion–tension couplings in the stiffnesses of the slant-cracked shaft. Therefore, combination frequencies $|\Omega - \omega_T|$ and $\Omega + \omega_T$ in the flexural responses and torsional excitation frequency ω_T in the axial response are very easy to be identified for the slant-cracked shaft, while they are not for the transverse-cracked shaft.

5. Experiment introduction

In order to testify the numerical results, an experiment is conducted. Schematic diagram of experimental setup is shown in Fig. 7. Shaft and disk are parts of the rotor system. When the rotor rotates, the torsional equipment composed of sliding blocks, mounting boards, electromagnets and ferroferrites will exert the torsional excitation on the disk. Connection between mounting board with sliding block and electromagnet is screw fastening. The electromagnet becomes magnetic when the electric current is switched on, and the magnetic force makes the electromagnet and the ferroferrite attract each other. Because the ferroferrites are fixed with the foundation, the electromagnets have to move and consequently drive two sliding blocks to hold the disk. When the rotor rotates, the frictional force between the sliding blocks and disk produces the rotor system torsional excitation. Function generator can output a sinusoidal signal with a constant frequency. After being amplified by the power amplifier, the enhanced signal voltage will drive the electromagnet to control the torsional excitation. An eddy-current transducer is used to measure the horizontal vibration displacements of the shaft.

The experimental setup is shown in Fig. 8. The rated current of the electromotor is 2.5 A and the output power is 250 W. The rotating speed can be adjusted between 0 and 10 000 rev/min and the rate of raising speed

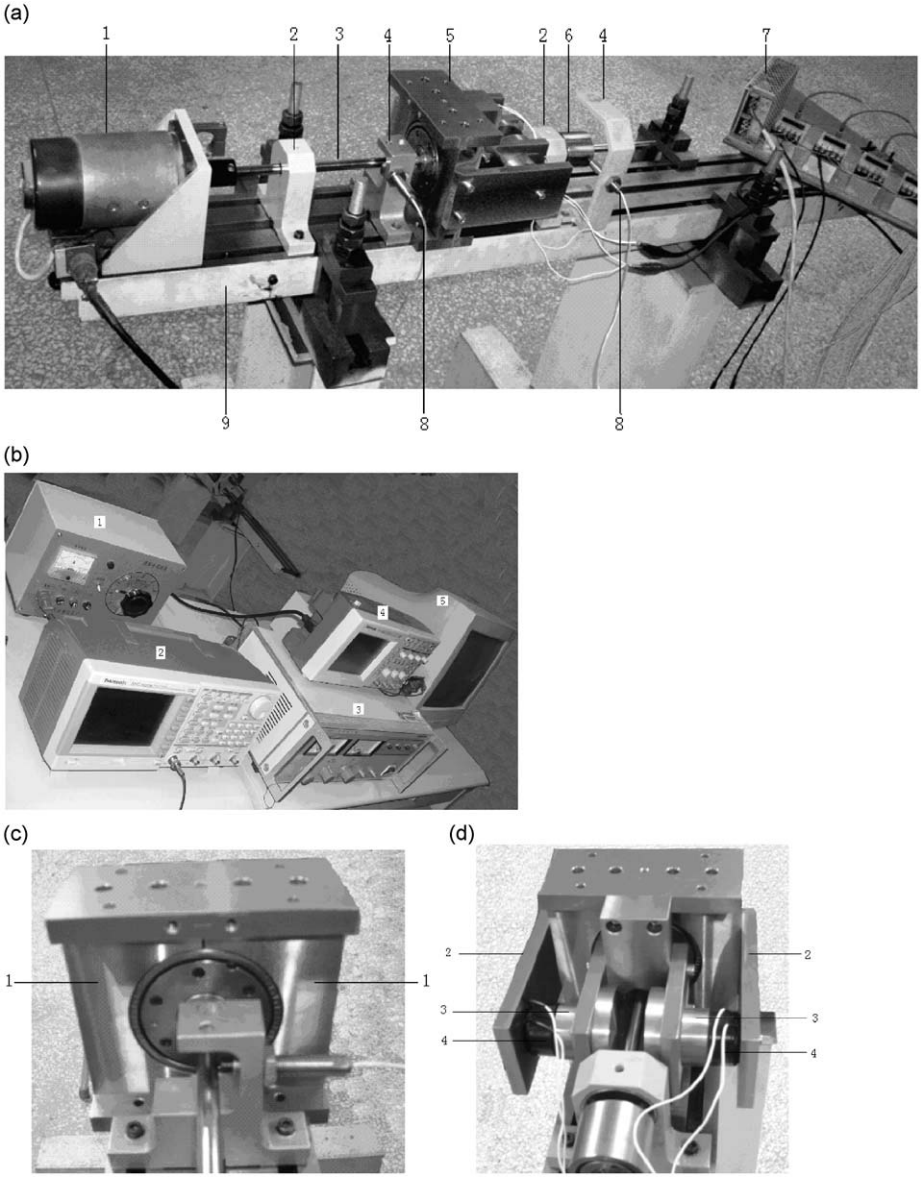

Fig. 8. Experiment setup of the rotor system with a torsional equipment: (a) (1) electromotor, (2) pedestal, (3) cracked shaft, (4) transducer holder, (5) torsional equipment, (6) key phaser, (7) pre-processor, (8) eddy-current transducer, and (9) foundation, (b) (1) speed governor, (2) function generator, (3) power amplifier, (4) oscillograph, and (5) computer, (c) (1) sliding block, and (d) (2) mounting board, (3) ferroferrite, and (4) electromagnet.

can reach up to 800 rev/min. Even so, during experiment the rotating speed is always controlled under 4000 rev/min. Because when there is a deep crack on the shaft, strong vibrations are very dangerous once the rotating speed is above 4000 rev/min for the experimental rotor. A semi-flexural coupling is used to connect the electromotor and the shaft. The diameter of the shaft is 9.5 mm and the length of the shaft is 500 mm. During experiment, there are two shafts to change, one with a transverse crack and the other with a 45° slant crack, as shown in Fig. 9. The crack would be always open since it is cut by a linear cutting machine with the diameter of molybdenum filament 0.18 mm. The depth is 4 mm for both cracks: transverse and slant. The 0.18 mm thick slot is used to simulate the fully open crack, not the breathing crack. Since the main characteristic frequencies are same for the responses of the shaft with a fully open crack and with a breathing crack, and the fully open crack can be produced more easily by machining a slot, it is feasible to take the slot

Fig. 9. Transverse-cracked shaft and 45° slant-cracked shaft.

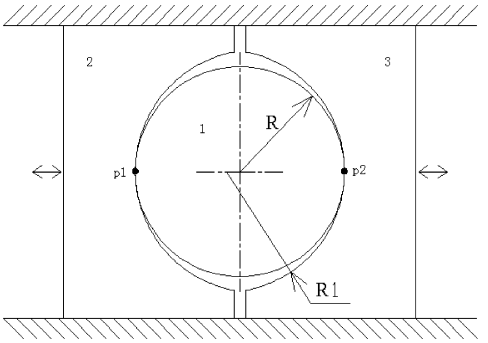

Fig. 10. Schematic diagram of disk 1 and sliding blocks 2 and 3.

as the open crack to study the vibrations of the cracked shaft. This is why the vibrations of the shaft with the fully open crack are investigated in the last section of flexural steady-state responses. The effective support distance between two pedestals is about 260 mm. The disk is in the middle of the effective support distance and the crack on the shaft is adjacent to the disk. The mass of the disk is 612.8 g and the diameter is 76 mm. Fig. 10 displays the relative position of the sliding blocks and the disk. The sliding blocks can move smoothly along a fixed bottom board, and their circular arcs contact tangentally with the excircle of the disk when two sliding blocks hold the disk, as shown in Fig. 10.

Acquired signal from eddy-current transducer is voltage with the range: $-5\sim5$ V. The distance range between the top of the eddy-current transducer and the measured surface 0–2 mm is corresponding to the voltage range. In this section, all amplitudes of experimental results are denoted by voltage V.

Fig. 11(a) is a sinusoidal signal that is outputted directly from the function generator. Its frequency is 15 Hz. However, once this signal is converted into the torsional excitation by the electromagnet, the frequency of the torsional excitation changes into 30 Hz, as shown in Fig. 11(b). Because the attractive force between the electromagnet and the ferroferrite is only related to the absolute magnitude of the signal current no matter which direction of the current is. Naturally, in order to drive the electromagnet better and produce a proper attractive force, the amplitude of the signal from the function generator will be amplified by the power amplifier before the signal is inputted into the electromagnet, not just 5 V as shown in Fig. 11(b). In this experiment, the amplitude of the amplified signal inputted into the electromagnet is 20 V.

Figs. 12(a)–(i) and 13(a)–(i) display the experimental spectra of the horizontal responses of the transverse-cracked and slant-cracked shafts with increase of the rotating speed under the torsional excitation. In these spectra, Ω is rotating speed, $\omega_T = 30\,\text{Hz} = 1800\,\text{rev/min}$ is the frequency of torsional excitation, denotations $\ominus$ and $\oplus$ represent spectrum lines of $|\Omega - \omega_T|$ and $\Omega + \omega_T$, respectively, and $\circ$ represents spectrum line of twice power frequency. In China, power frequency is 50 Hz. The power frequency is brought forth by the power amplifier, and the frequency becomes twice after it is converted into the torsional excitation just like the signal from the function generator happens. Therefore, there is always a twice power frequency $f_e = 100$ Hz, i.e. 6000 rev/min, in every spectra of experimental horizontal responses.

In Figs. 12 and 13, rotating speed Ω, its second harmonic frequency 2Ω, frequency of torsional excitation ω_T, twice power frequency f_e and combination frequencies $|\Omega - \omega_T|$ and $\Omega + \omega_T$ are marked clearly. It can be seen that frequencies Ω, 2Ω, and ω_T are all obvious in the horizontal responses whether for the

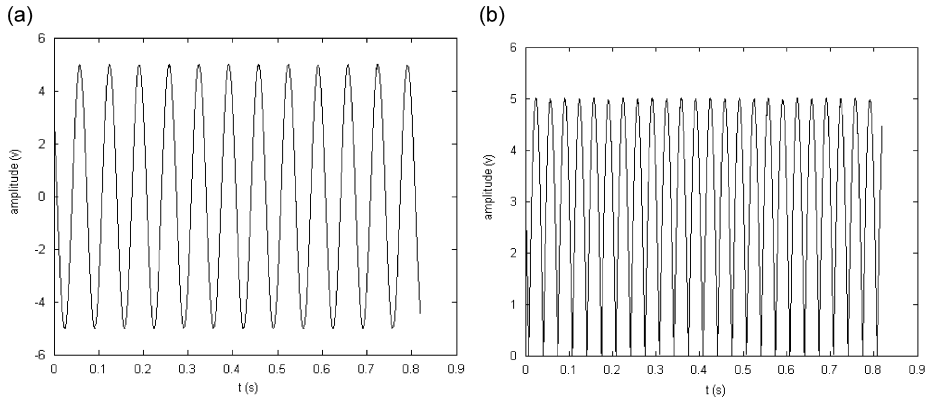

Fig. 11. (a) Signal from function generator and (b) schematic signal of torsional excitation frequency.

transverse-cracked shaft or the slant-cracked one. However, combination frequencies $|\Omega - \omega_T|$ and $\Omega + \omega_T$ are evident only for the slant-cracked shaft. For the transverse-cracked shaft, they are too small to be visible especially when the rotating speed is low. With the rotating speed increasing, more combination frequencies arise for both shafts, and the horizontal responses of the slant-cracked shaft demonstrate far stronger coupling vibrations than those of the transverse-cracked shaft. This can be illustrated by Fig. 12(j), which is enlarged to almost the same dimension as Fig. 13(i). In Fig. 12(j), except for the marked spectrum lines, there exist other four obvious lines denoted by 1–4. Corresponding frequencies of these four spectrum lines are: (1) $2\omega_T - \Omega$, (2) $2\omega_T$, (3) $2\Omega - \omega_T$, and (4) $3\omega_T$, respectively. Contrast between Figs. 13(i) and 12(j) shows that despite the similar higher rotating speeds, amplitudes of combination frequencies in the responses of the transverse-cracked shaft is much smaller than those in the responses of the slant-cracked one. The contrast is sharper when the rotor rotates at a low speed. Due to frequencies f_e and ω_T existing in the torsional excitation, many other combination frequencies would arise also. For example, in Fig. 13(j), there are several remaining obvious frequencies denoted by 1–7 appearing in the spectrum. They are: (1) $f_e + 3\omega_T - 4\Omega$, (2) $3\Omega - \omega_T - f_e$, (3) $2\omega_T - \Omega$, (4) $2\Omega + \omega_T - f_e$, (5) $f_e - \Omega$, (6) $2\omega_T$, and (7) $f_e - \omega_T$, respectively. For other spectra of the horizontal responses in Figs. 12 and 13, the remaining frequencies are similar to those in Fig. 13(j), almost all of which are combination frequencies of ω_T, f_e, and Ω. Only these combination frequencies are much more prominent in the horizontal responses of the slant-cracked shaft.

In numerical results as shown in Fig. 5, the amplitude of main frequency Ω in the horizontal responses for the transverse-cracked shaft is about twice as large as that for the slant-cracked shaft. However, in experimental results as shown in Figs. 12 and 13, it is about four times. The reason might be that the torsional excitation is exerted by direct contact of mechanical structure. The contacting of sliding blocks with disk restricts the displacement of the shaft in the horizontal response to some extent. While the whole system rotates steadily under the torsional excitation, there will be a constant torque whether for the slant-cracked rotor or the transverse-cracked rotor. Because the frequency 30 Hz of torsional excitation is high enough, sliding blocks barely have time to loosen the disk totally due to the sliding resistance. The difference between the left sliding resistance and the right one will lead to a slight horizontal force on the shaft, which is the term $A\sin(\omega_T t)$ in Eq. (2). Since the flexural response of the slant-cracked shaft is less than that of the transverse-cracked shaft when there is no torsional excitation, the force to resist the sliding resistance for the slant-cracked shaft is not as strong as that for the transverse-cracked shaft, and the sliding blocks would hold the disk of the slant-cracked rotor much tighter. Therefore, the restriction limits the horizontal response of the slant-cracked shaft more heavily. This results in the amplitude differences between numerical results and experimental results. On the other hand, the restriction caused by direct contact of mechanical structure also make the second harmonic frequency 2Ω seemingly strong in the spectra of experimental horizontal responses. Numerical results show that the amplitude of main frequency Ω is always larger than that of 2Ω and with increase of rotating speed, the amplitude of Ω increases much faster than that of 2Ω. In this case, when two sliding blocks hold the disk in the experiment, the amplitude of Ω will be firstly and heavily restricted and

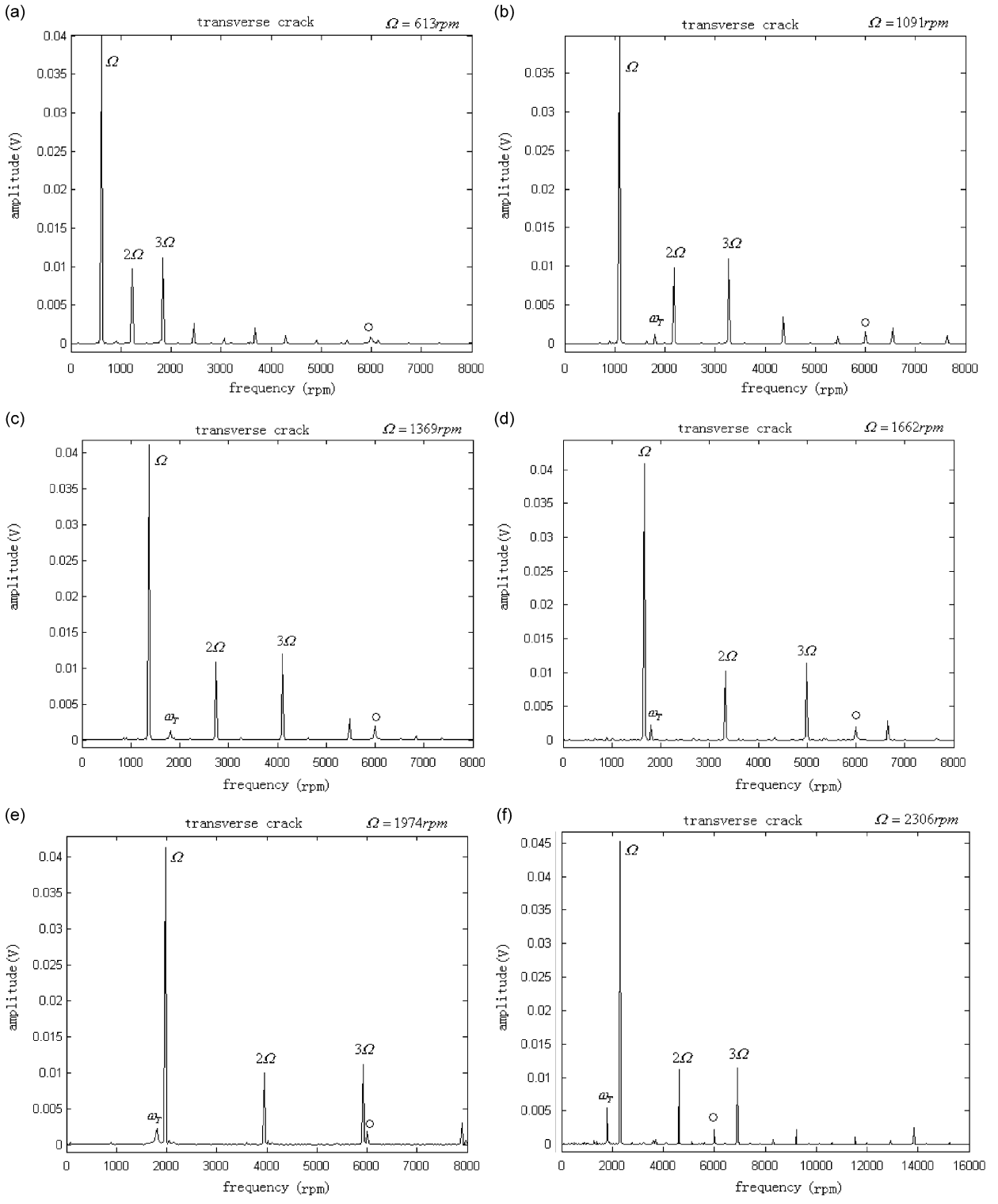

Fig. 12. Experimental spectra of the horizontal responses of the transverse-cracked shaft with increase of the rotating speed under torsional excitation.

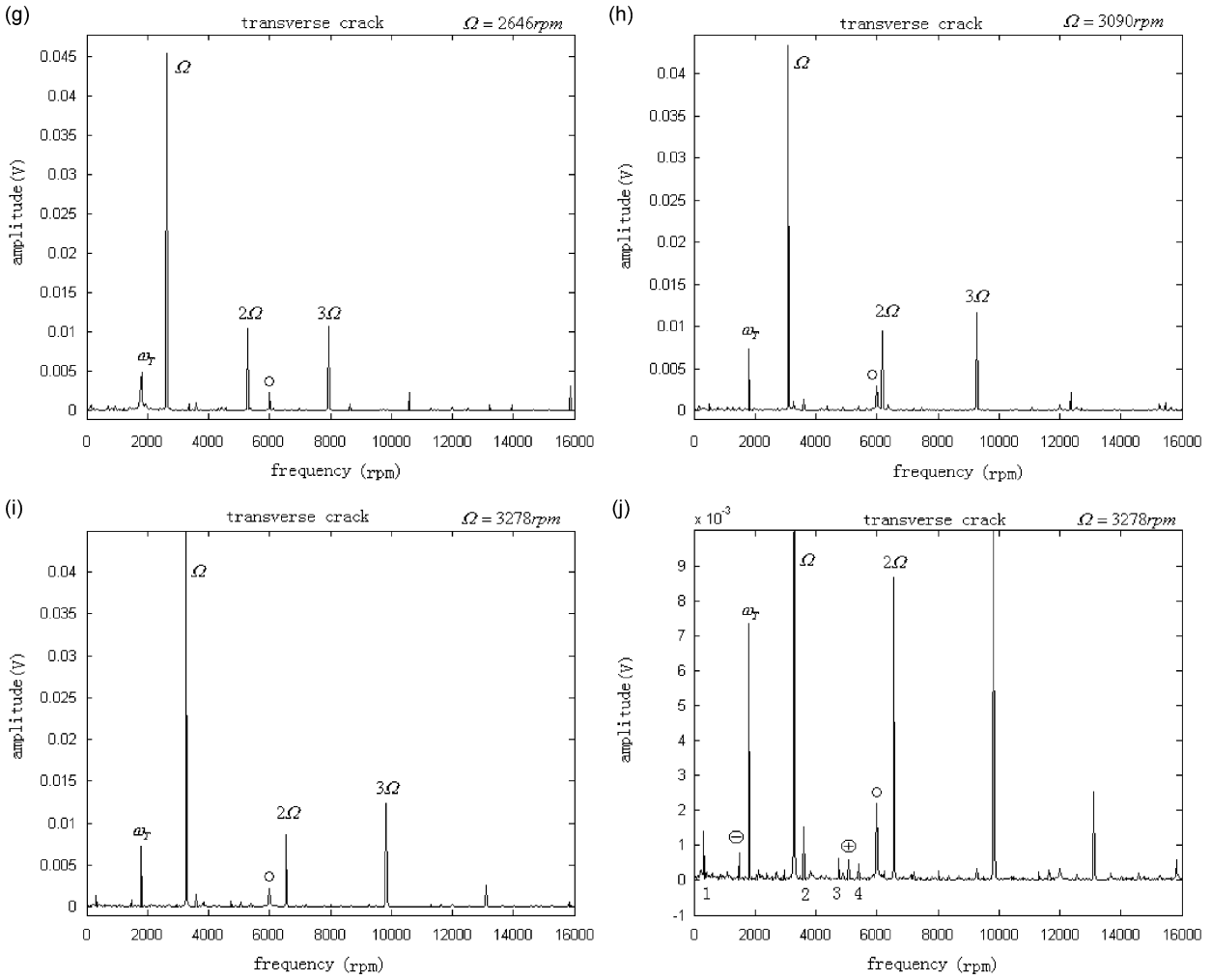

Fig. 12. (*Continued*)

decreased. In contrast, the amplitude of 2Ω will be influenced much less. Therefore, frequency 2Ω looks strong in the spectra of the experimental results. In fact, the direct contacting way of the equipment is also the main reason that experimental responses contain more combination frequencies than numerical responses.

6. Conclusions

Flexural vibrations of the cracked rotor system with a transverse crack or a slant crack on the shaft have been investigated considering the torsional excitation. Numerical results and experimental results are obtained and analyzed.

In order to solve the motion equations, stiffnesses of the cracked shaft are derived firstly. The derivation shows that there are bending–torsion–tension coupling stiffnesses for the slant-cracked shaft, however only bending–tension coupling stiffnesses for the transverse-cracked shaft. Fundamental reasons are that the bending, torsional, and tensional loads all can make the slant crack be the I mode crack, however only bending and tensional loads can make the transverse crack be the I mode crack.

Eccentricity can lead to bending–torsion coupling vibrations whether for the transverse-cracked shaft or the slant-cracked one. Since there have existed the bending–tension coupling vibrations caused by bending–tension coupling stiffnesses for the transverse-cracked shaft, there would be bending–torsion–tension coupling

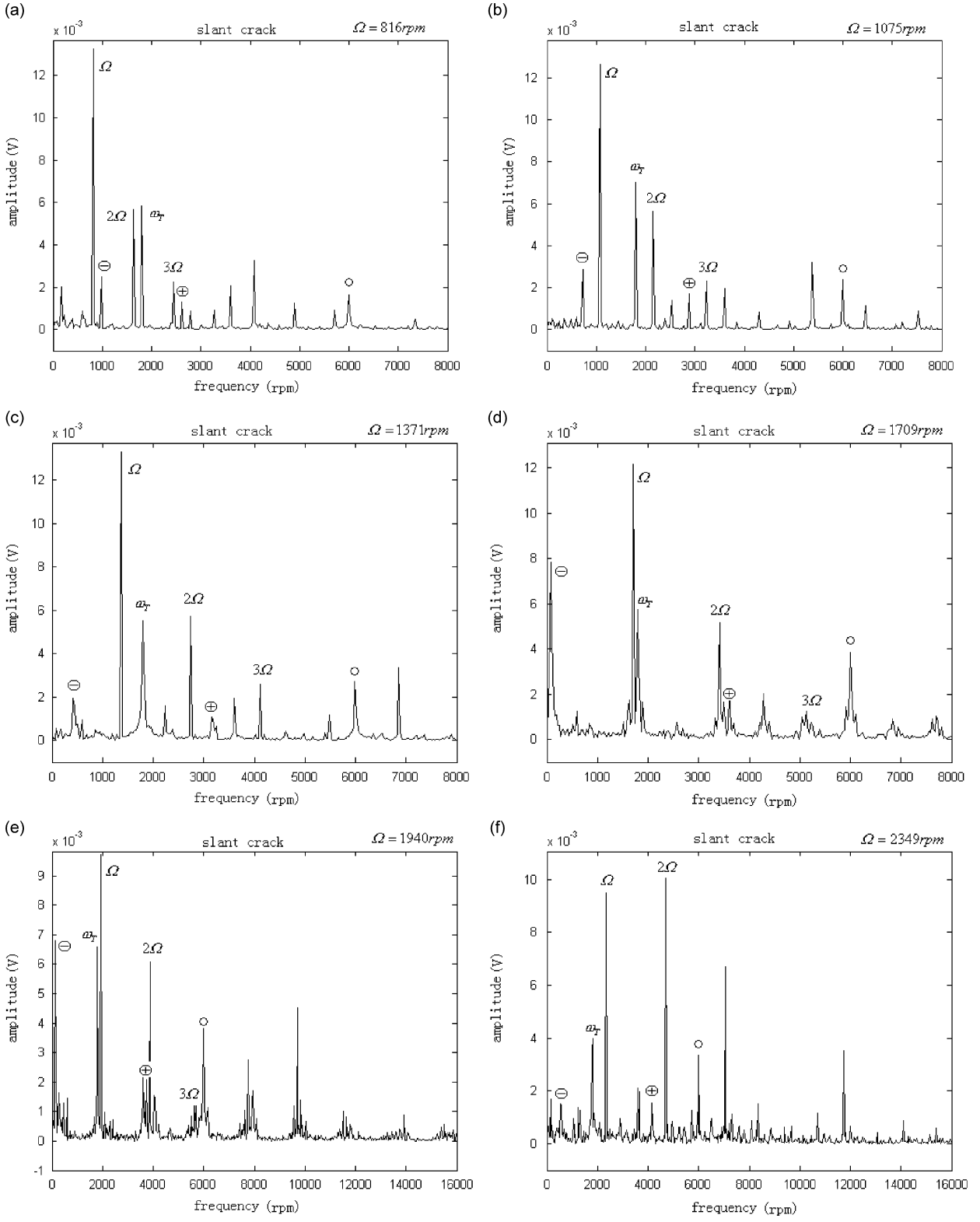

Fig. 13. Experimental spectra of the horizontal responses of the slant-cracked shaft with increase of the rotating speed under torsional excitation.

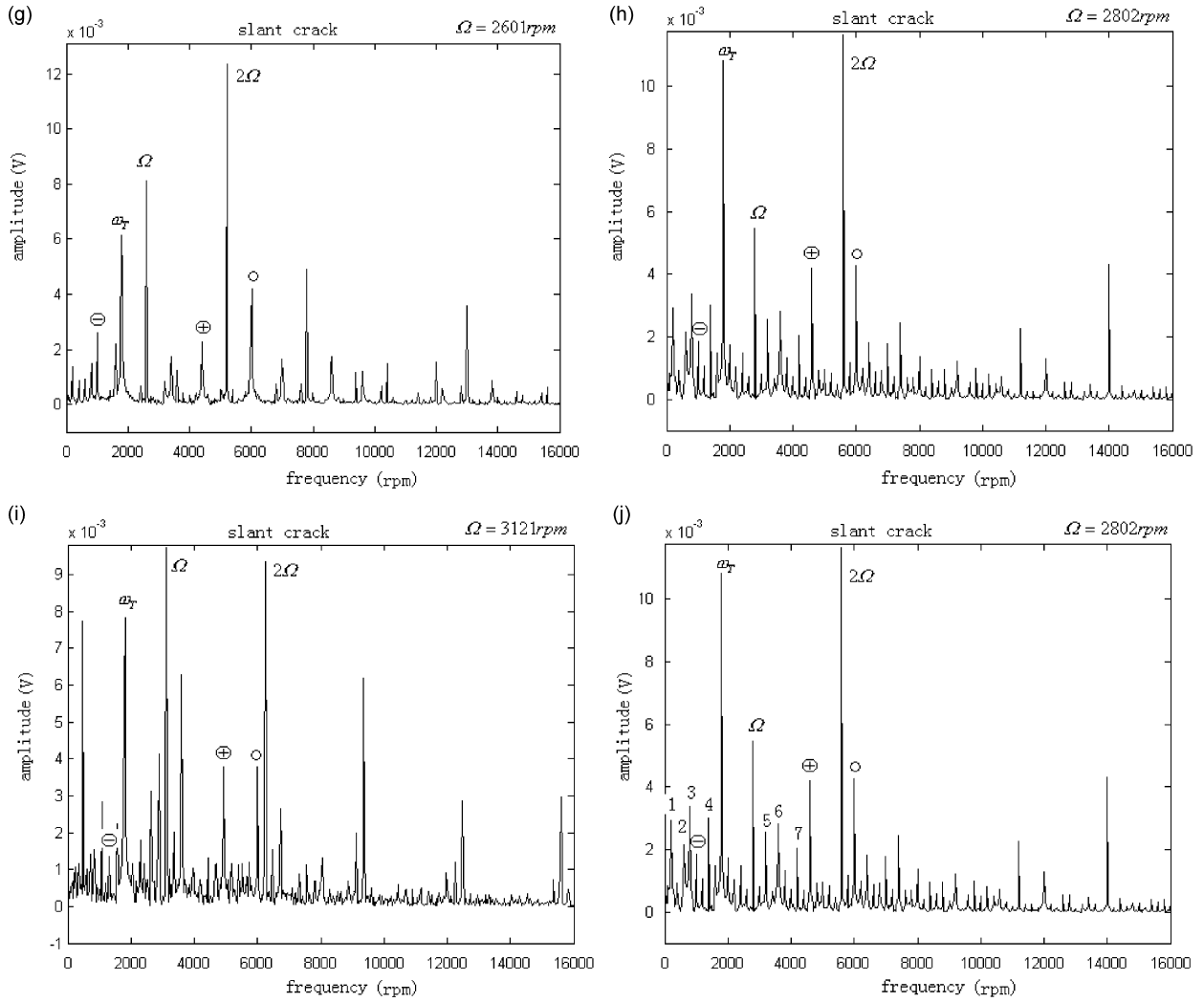

Fig. 13. (*Continued*)

vibrations in the responses of the transverse-cracked rotor system due to the interaction of couplings. Even so, the slant-cracked shaft demonstrates much stronger coupling vibrations than the transverse-cracked shaft, because there originally exist the bending–torsion–tension coupling vibrations caused by bending–torsion–tension coupling stiffnesses for the slant-cracked shaft.

Comparison of numerical results between the responses of the transverse-cracked shaft and those of the slant-cracked shaft demonstrates that combination frequencies $|\Omega - \omega_T|$ and $\Omega + \omega_T$ in the flexural responses and torsional excitation frequency ω_T in the axial response are very easy to be identified for the slant-cracked shaft, but not for the transverse-cracked shaft. Comparison of experimental results testifies that combination frequencies $|\Omega - \omega_T|$ and $\Omega + \omega_T$ are indeed much more prominent in the flexural responses of the slant-cracked shaft than those in the flexural responses of the transverse-cracked shaft, especially when the rotor rotates at a low speed. Experimental results also present evidence that the slant-cracked shaft indeed behaves much stronger coupling vibrations than the transverse-cracked shaft.

Therefore, combination frequencies $|\Omega - \omega_T|$ and $\Omega + \omega_T$ in the flexural responses can be used to discriminate between the slant crack and the transverse crack on the shaft, and the best speed range of application is under the natural frequency of the rotor. The lower rotating speed is, the easier distinguishing between the slant crack and the transverse crack by combination frequencies is. Analysis of numerical results

indicates that torsional excitation frequency ω_T appearing in the axial response could be another important characteristic which can be used to discriminate between the slant crack and the transverse crack at any rotating speed. This needs to be validated by more experimental investigations.

Acknowledgments

This work was supported by Natural Science Foundation of China (Grant nos. 50425516 and 10732060) and the National High Technology Research and Development Program of China (863 Program) (no. 2006AA04Z438).

References

[1] A.D. Dimarogonas, *Dynamic Response of Cracked Rotors. Technical Information Series*, General Electric Co., Schenectady, NY, 1970.
[2] T. Pafelias, *Dynamic Behavior of a Cracked Rotor. Technical Information Series*, General Electric Co., Schenectady, NY, 1974 No. DF-74-LS-79.
[3] A.D. Dimarogonas, Vibration of cracked structures: a state of the art review, *Engineering Fracture Mechanics* 55 (5) (1996) 831–857.
[4] S. Zhaohong, et al., Classic Malfunction Analysis of the Aeroengine, BUAA Press, 1993, p. 3.
[5] M. Ichimonji, S. Watanabe, The dynamics of a rotor system with a shaft having a slant crack, *JSME International Journal, Series III* 31 (4) (1988) 712–718.
[6] M. Ichimonji, Y. Kazao, S. Watanabe, S. Nonaka, The dynamics of a rotor system with a slant crack under torsional vibration, *Nonlinear and Stochastic Dynamics* 78 (1994) 81–89.
[7] A.S. Sekhar, P.B. Prasad, Dynamic analysis of a rotor system considering a slant crack in the shaft, *Journal of Sound and Vibration* 208 (3) (1997) 457–474.
[8] A.S. Sekhar, A.R. Mohanty, S. Prabhakar, Vibrations of cracked rotor system: transverse crack versus slant crack, *Journal of Sound and Vibration* 279 (2005) 1203–1217.
[9] A.K. Darpe, Dynamics of a Jeffcott rotor with slant crack, *Journal of Sound and Vibration* 303 (1–2) (2007) 1–28.
[10] A.K. Darpe, Coupled vibrations of a rotor with slant crack, *Journal of Sound and Vibration* 305 (1–2) (2007) 172–193.
[11] A.D. Dimarogonas, S.A. Paipetis, *Analytical Methods in Rotor Dynamics*, Applied Science Publishers, London, 1983.
[12] H. Tada, P.C. Paris, G.R. Irwin, *The Stress Analysis of Cracks Handbook*, third ed., Professional Engineering Publishing, 2000.
[13] O.S. Jun, H.J. Eun, Modelling and vibration analysis of a simple rotor with a breathing crack, *Journal of Sound and Vibration* 155 (2) (1992) 273–290.